Progress In Electromagnetics Research C, Vol. 70, 33–41, 2016

A Printed Wideband MIMO Antenna System for GSM1800/1900, UMTS, WLAN2450, LTE2300/2500, and GPS Applications

Mohamed M. Morsy*

Abstract—A low-profile wideband multiple-input-multiple-output (MIMO) antenna is presented. The proposed antenna is suitable for mobile terminals applications as its measured −10 dB bandwidth ranges from 1.56 GHz to 2.77 GHz. The overall antenna efficiency ranges from 68% to 83% over the operating bandwidth. The overall size of the proposed antenna is $60 \times 97 \times 0.8\,\text{mm}^3$. A novel isolation structure is employed to achieve isolation range of −26 dB to −16 dB. The radiation patterns are measured, and envelope correlation coefficient is evaluated. The simulated and measured results are in good agreement.

1. INTRODUCTION

Multiple input multiple output (MIMO) antennas are used to improve wireless communication capacity and effectiveness by using the techniques of multipath [1]. A lower envelope correlation of MIMO antennas is required in order to mitigate the multipath interference problem. Recently, there has been a high demand on efficient mobile wireless communications that require high transfer rate and high capacity. The performance of microstrip monopole antennas has proven to be very promising in designing multiband and wideband antennas for MIMO systems [1–5]. Good isolation between the MIMO antenna elements is a necessity in order to correctly transmit and receive uncorrelated signals. However, it is challenging to integrate multiple antennas in a confined space in mobile terminals while maintaining good isolation. Theoretically, antenna elements require more than half of a wavelength separation to achieve good isolation [6]. Many techniques have been used for decoupling MIMO antenna elements while maintaining miniaturized elements. Isolation improvement structures can substantially enhance the isolation of the MIMO antenna elements [1, 2]. In [1], an isolation improvement structure is added between antenna elements to achieve isolation less than −20 dB, while in [2], a slit is added in the ground plane between the two MIMO elements to improve the isolation of the elements. In [7], an isolation structure, formed by parasitic elements, is attached to the ground plane in order to achieve high isolation. In [8], a protruded ground plane is employed as an isolation structure, while in [9], a parasitic element is inserted between two radiating elements to enhance their port-to-port isolation. Radiation pattern diversity technique has also proven to be an effective method for achieving highly isolated MIMO elements as illustrated in [3] and [10].

In this paper, a unique ground plane structure is implemented in order to improve the isolation between the antenna elements by adding an isolation structure that disturbs the surface current between the antenna elements, and hence increasing the isolation between radiating elements. Furthermore, the antenna is designed for mobile terminals, as it covers a wide range of 3G/4G frequencies such as GPS (1575.42 MHz), GSM1800/1900 (1710–1880 MHz and 1850–1990 MHz), UMTS (1920–2170 MHz), WLAN2450, LTE2300/2500 Applications.

Received 30 September 2016, Accepted 22 November 2016, Scheduled 6 December 2016

* Corresponding author: Mohamed M. Morsy (mmorsy@pmu.edu.sa).

The author is with the Electrical Engineering Department (ABET Accredited Program), Prince Mohammad Bin Fahd University (PMU), Al Khobar 31952, Kingdom of Saudi Arabia.

2. ANTENNA CONFIGURATION

The geometry of the proposed MIMO antenna is shown in Figure 1. The antenna prototype consists of two E-like microstrip monopole elements that are printed on both sides of FR4 with permittivity 4.4 and height 0.8 mm. The total size of the antenna is $97 \times 60\,\text{mm}^2$. The two antenna elements are separated by a distance of 22 mm which is almost equivalent to one-tenth of the wavelength of the lowest resonant frequency. The feeding network along with truncated ground plane is designed to achieve 50-Ω characteristic impedance over the operating frequency band. The optimized dimensions of the prototype antenna are shown in Table 1. The radiating E-like elements are backed with an isolation structure attached to the ground plane of the antenna in order to improve isolation between radiating elements.

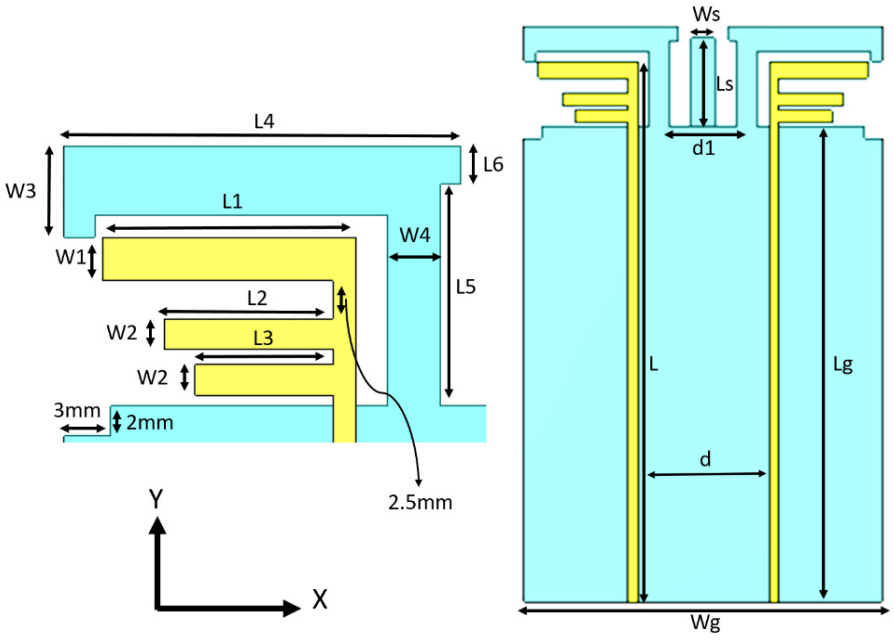

Figure 1. Geometry of the proposed MIMO antenna.

Table 1. Optimized parameters of the proposed MIMO antenna.

Parameter	Value (mm)	Parameter	Value (mm)
Lg	22	Wg	60
L	91	d	22
$L1$	16.5	$W1$	2.8
$L2$	11	$W2$	2
$L3$	9	$W3$	6
$L4$	25.8	$W4$	3.5
$L5$	14.5	$d1$	11
$L6$	6	Ws	4
Ls	15		

3. RESULTS AND PARAMETRIC ANALYSES

The performance of the proposed antenna depends on proper dimensions of radiating elements along with the truncated ground plane in order to achieve good matching over the operating frequency band. To gain insight into how proposed antenna works, the effects of the background isolation structure are analyzed. The use of isolation structure has been validated as illustrated in Figure 2, which shows the effect of the isolation structure on the return loss and isolation of the two elements MIMO antenna.

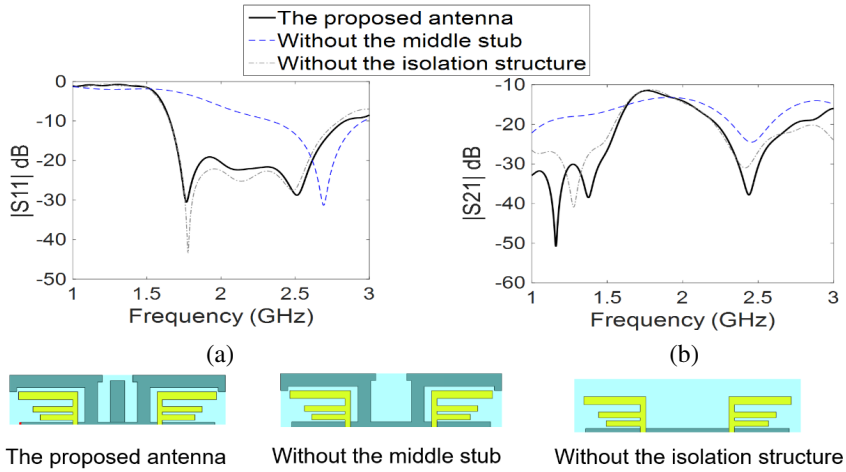

Figure 2. Simulated $|S11|$ and $|S21|$ of three different cases; the optimized proposed antenna, the proposed antenna without the ground plane stub, and the proposed antenna without the isolation structure.

As illustrated in Figure 2, three cases are considered. Case 1 is analyzed without the isolation structure, and case 2 is analyzed without the middle stub in the isolation structure, while case 3 is analyzed with the complete isolation structure. It is seen that the -10 dB impedance bandwidth is wider for case 2 and case 3, while it is narrow for case 1, as illustrated in Figure 2(a). It is noticed that case 2 and case 3 feature the better isolation performance; however case 3 provides better isolation in higher frequencies of the operating frequency band. It is seen that the -10 dB impedance bandwidth is wider for case 2 and case 3, while it is narrow for case 1, as illustrated in Figure 2(a). Figure 2(b) shows the effect of the three aforementioned cases on $|S21|$. It is noticed that case 2 and case 3 feature good isolation performance; however, case 3 provides better isolation in higher frequencies of the operating frequency band. It is noticed that case 2 and case 3 have similar results ($S11$ and $S21$ curves); however, case 2 is merely an intermediate stage between having no isolation structure (Case 1) and having an optimized isolation structure (Case 3). It is seen that the isolation structure not only provides good isolation between elements, but also works as a matching element to the radiating elements.

For further study of the functionality of the proposed MIMO antenna, the surface current distributions are investigated at 1.8 GHz, 2.4 GHz, and 2.6 GHz as illustrated in Figure 3. It is shown that the feedline has two maximum values and a null value along the feedline as shown in Figure 3(a), while in Figures 3(b) and 3(c), the feedline has almost three maximum values and two null values. Therefore, it is apparent that the current distributions at the upper resonances, 2.4 GHz, and 2.6 GHz, are in higher harmonic order than the current distribution at the lower resonant frequency, 1.8 GHz.

An understanding of the role of the isolation structure can be secured by comparing the surface current distributions of the optimized design (with isolation structure), shown in Figure 3, with their corresponding current distributions of the designed antenna and without the isolation structure, as displayed in Figure 4. It is seen that without the isolation structure, a significant amount of surface current flows between antenna elements as displayed in Figure 4. On the contrary, the surface current, flowing between the two MIMO antenna elements, is substantially reduced in presence of the isolation structure as shown in Figure 3.

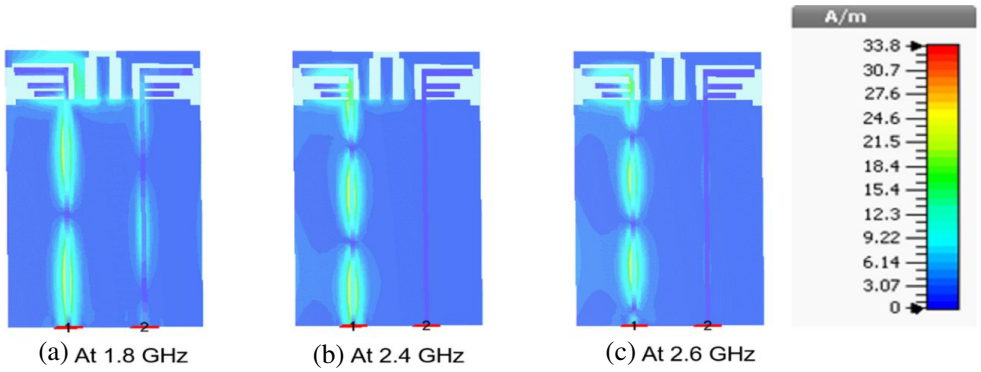

Figure 3. Surface current distribution (A/m) for the optimized design: (a) at 1.8 GHz, (b) at 2.4 GHz, and (c) at 2.6 GHz.

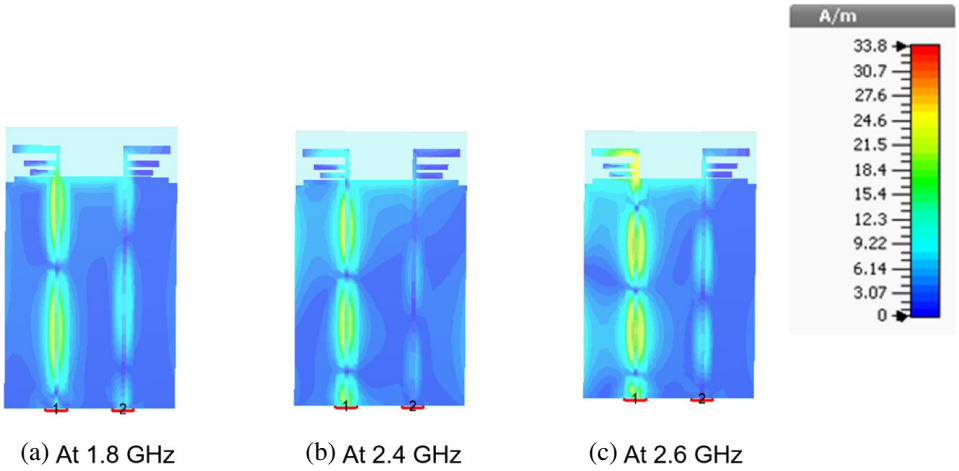

Figure 4. Surface current distribution (A/m) for the designed antenna (without the isolation structure): (a) at 1.8 GHz, (b) at 2.4 GHz, and (c) at 2.6 GHz.

The scattering parameters, commonly known as S-parameters, come from the "Scattering Matrix" [11]. Equation (1) represents the S-parameters equation of the model described in Figure 5.

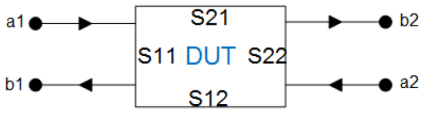

Figure 5. Two ports S-parameter model.

$$b1 = S11\,a1 + S12\,a2, \quad b2 = S22\,a2 + S21\,a1 \tag{1}$$

It is seen that terminating the DUT in the characteristic impedance (Zo) allows the extraction of the individual S-parameters ($S11$ or $S22$). For instance, if the characteristic impedance (Zo) is equal to 50-Ω, and a 50-Ω termination is present at port 2, $a2$ is reduced to zero, resulting in Equation (2).

$$S11 = \left.\frac{b1}{a1}\right|_{a2=0} \tag{2}$$

Figure 6. A photograph of the fabricated prototype MIMO antenna.

Similarly, terminating port 1 by a 50-Ω load, $a1$ is reduced to zero, resulting in equation for $S22$ as shown in Equation (3).

$$S22 = \left.\frac{b2}{a2}\right| a1 = 0 \tag{3}$$

Figure 6 shows the fabricated (2 × 1) MIMO antenna prototype. The simulated and measured S-parameters for the designed antenna are displayed in Figure 7, where $|S11|$ is obtained by exciting one port of the two elements MIMO antenna system, while terminating the other element to a 50-Ω load. Because of the symmetry of the two antenna elements, only $|S11|$ and $|S21|$ curves are given. Theoretically, $|S22|$ and $|S12|$ curves are identical to $|S11|$ and $|S21|$ curves, respectively. Figure 7 shows that the simulated −10 dB impedance bandwidth ranges from 1.65 GHz to 2.83 GHz, with simulated $|S21|$ less than −12 dB over the same frequency band, while the measured −10 dB impedance bandwidth ranges from 1.56 GHz to 2.77 GHz. The measured $|S12|$ ranges from −26 dB to −16 dB over the operating bandwidth 1.65 GHz to 2.83 GHz. The discrepancy between the measured and simulated results is attributed to the low-quality FR4 PCB and the fabrication process that relies mainly on chemical etching rather than PCB mechanical milling machine, which produces much accurate printout. For example, the measured and simulated isolation ($|S12|$) curves are summarized in Table 2. It is seen that over the frequency range, 1.6–2.1 GHz, the measured isolation is better than simulated one. However, the simulated isolation is much better than the measured one over the frequency range, 2.1–2.5 GHz. For the frequency range, 2.5–2.77 GHz, there is a subtle difference between the measured and simulated isolation curves.

Table 2. Comparison between the measured and simulated isolation range over frequency band, 1.6–2.77 GHz.

Frequency Band	**Simulated Isolation range, $S12$ (dB)**	**Measured Isolation range $S12$ (dB)**
1.6–2.1 GHz	−18.8 to −11.5	−20.7 to −15.8
2.1–2.5 GHz	−37.7 to −19	−25 to −19
2.5–2.77 GHz	−25 to −19	−26 to −22

The measured S-parameters show that the proposed MIMO antenna is compatible for GPS (1575.42 MHz), GSM1800/1900 (1710–1880 MHz and 1850–1990 MHz), UMTS (1920–2170 MHz), WLAN2450, and LTE2300/2500 applications.

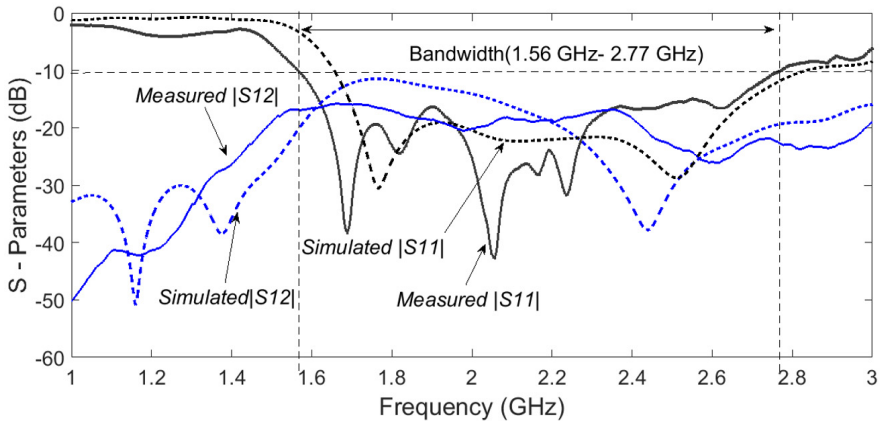

Figure 7. Simulated and measured S-parameters of the proposed MIMO antenna.

4. RADIATION PATTERN AND DIVERSITY PERFORMANCE

The radiation patterns of the proposed MIMO antenna are evaluated in an anechoic chamber where port 1 is excited while port 2 is terminated with 50-Ω load. Figures 8, 9 exhibit the theta- and phi-components of the radiation patterns at 1.8 GHz and 2.6 GHz in the x-y, y-z, and x-z planes. It is seen that the phi-component of the gain in x-y plane is almost close to the total gain since the theta-component of the gain is very small compared to the phi-component which indicates a linear polarization feature as shown in Figures 8(a) and 9(a). It is seen that the simulated and measured patterns at 1.8 GHz, and 2.6 GHz are in good agreement. The radiation patterns at 2 GHz and 2.4 GHz are not given since they are similar to those at 1.8 GHz, and 2.6 GHz, respectively.

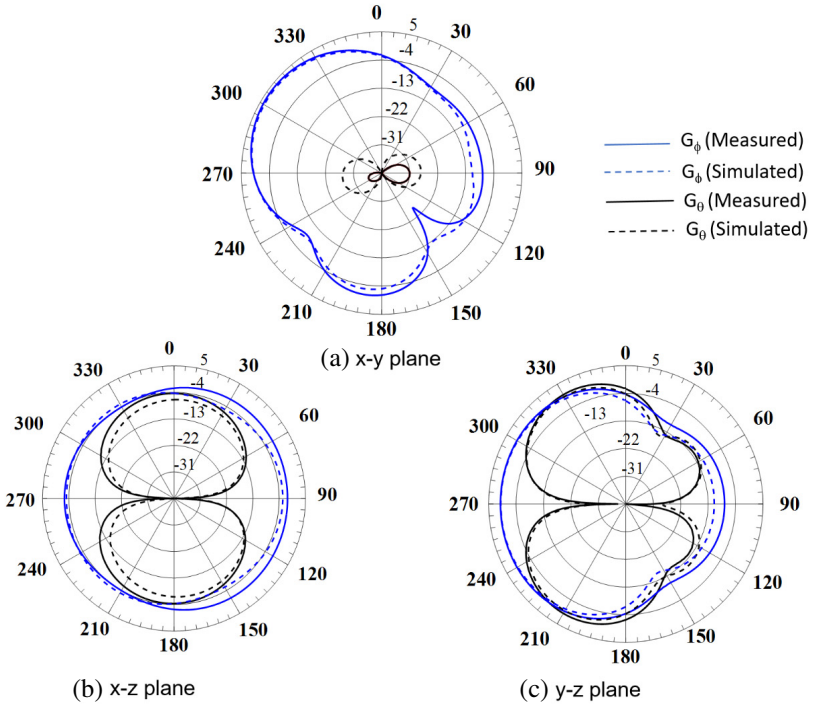

Figure 8. Theta- and phi-components of the radiation patterns at 1.8 GHz in the (a) x-y plane, (b) x-z plane, and (c) y-z plane.

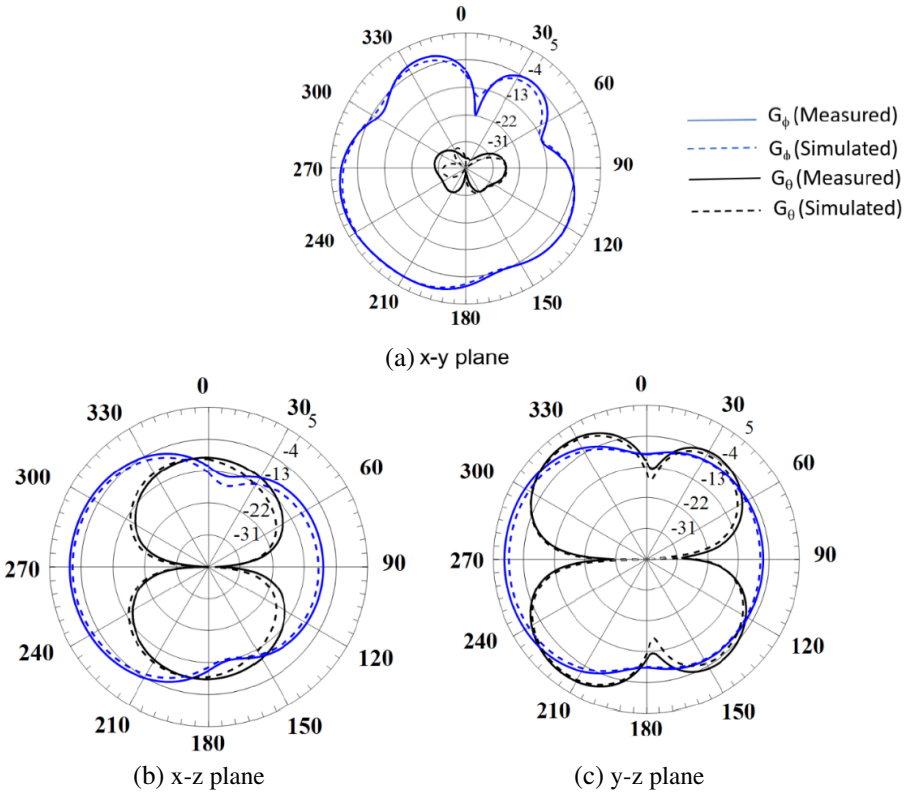

Figure 9. Theta- and phi-components of the radiation patterns at 2.6 GHz in the (a) x-y plane, (b) x-z plane, and (c) y-z plane.

The simulated peak gain and total efficiency of the proposed antenna are shown in Figure 10, where port 1 is exited and port 2 terminated with 50-Ω load. It is noticed that the peak gain varies from 0.25 dBi to 4.2 dBi over the operating frequency band (1.56 GHz–2.77 GHz). The total antenna efficiency is recorded to range from 68% to 83% over the operating frequency band.

Diversity gain is an important characteristic in a MIMO diversity antenna, and it can be obtained from the correlation coefficient. A good approximation of the relation between the diversity gain and the correlation coefficient can be obtained by the following formula [12]:

$$G_{app} \approx 10\sqrt{1-|\rho|^2} \tag{4}$$

where G_{app} is the apparent diversity gain. 10 dB is approximately the maximum apparent diversity gain. ρ is defined as the complex cross correlation coefficient and defined according to [13]:

$$|\rho|^2 \approx \rho_e \tag{5}$$

where ρ_e is the envelope correlation coefficient in terms of the S-parameter of the antenna system, and it can be expressed as [14]:

$$\rho_e = \frac{\left|S_{11}^* S_{21} + S_{12}^* S_{22}\right|^2}{\left(1-|S_{11}|^2+|S_{21}|^2\right)\ \left(1-|S_{11}|^2+|S_{12}|^2\right)} \tag{6}$$

If the correlation coefficient is close to unity, ρ is scaled by a scaling factor, 0.99, and Equation (4) becomes [12]:

$$G_{app} \approx 10\sqrt{1-0.99|\rho|^2} \tag{7}$$

The results of envelop correlation coefficient are in line with the simulated diversity gains at the operating frequency band which will guarantee a good diverse MIMO antenna system.

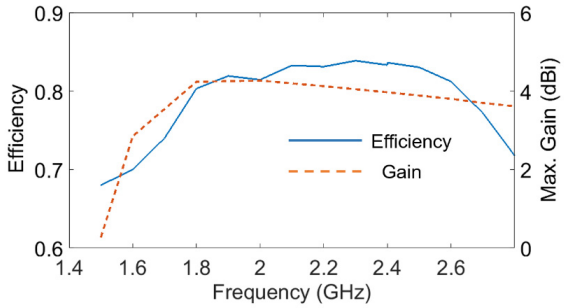

Figure 10. Simulated peak gain (dBi) and total antenna efficiency.

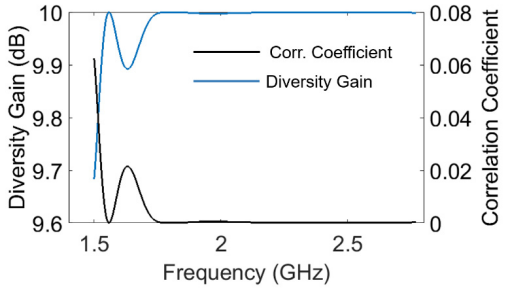

Figure 11. Evaluated envelope correlation coefficient and diversity gain of the proposed MIMO antenna.

The simulated envelope correlation coefficient and diversity gain of the proposed MIMO antenna system are displayed in Figure 11. The antenna exhibits good diversity gain that is greater than 9.7 dB over the operating frequency band (1.56–2.77 GHz). The results of the envelope correlation coefficient of the MIMO antenna is less than 0.07 over the same frequency band.

5. CONCLUSION

An MIMO antenna with a small size of $55 \times 58\,\text{mm}^2$ is proposed for a wideband operation. A prototype shows that the measured -10 dB impedance bandwidth is 1.2 GHz (1.57–2.77 GHz). The measured isolation is lower than -16 dB over the same frequency band. An isolation structure attached to the ground plane of the proposed antenna is employed in order to disturb the current distribution, and hence improve the decoupling between the antenna elements. The simulated total efficiency of the proposed antenna ranges from 68% to 83% over the operating frequency band. The diversity performance of the antenna system is investigated. Results show that the MIMO antenna can achieve an envelope correlation coefficient less than 0.07 across the operating frequencies. The simulated diversity gain is about 10 dB over the operating frequency band, which is in line with the calculated results of the envelope correlation coefficient. The surface current distribution and far-field gain are presented at operating frequencies.

REFERENCES

1. Jin, Z. J., J. H. Lim, and T. Y. Yun, "Frequency reconfigurable multiple-input multiple-output antenna with high isolation," *IET Microwaves, Antennas & Propagation*, Vol. 6, No. 10, 1095–1101, Jul. 17, 2012.
2. Wang, Y. and Z. Du, "A printed dual-antenna system operating in the GSM1800/GSM1900/UMTS/LTE2300/LTE2500/ 2.4-GHz WLAN bands for mobile terminals," *IEEE Antennas and Wireless Propagation Letters*, Vol. 13, 233–236, 2014.

3. Li, W. W., B. Zhang, J. H. Zhou, and B. Q. You, "High isolation dual-port MIMO antenna," *Electronics Letters*, Vol. 49, No. 15, 919–921, Jul. 18, 2013.
4. Morsy, M. M., M. A. Basha, and M. R. Khan, "Multi-band MIMO antenna for wireless devices," *Proceedings of the 2012 IEEE International Symposium on Antennas and Propagation*, 1–2, Chicago, IL, 2012.
5. Kadu, M. B., S. B. Deosarkar, and R. P. Labade, "Dual band microstrip patch antenna for MIMO system," *2015 International Conference on Pervasive Computing (ICPC)*, 1–4, Pune, 2015.
6. Carrasco H., H. D. Hristov, R. Feick, and D. Cofre, "Mutual coupling between planar inverted-F antennas," *Microwave Opt. Technol. Lett.*, Vol. 42, 224–227, 2004.
7. Toktas and A. Akdagli, "Wideband MIMO antenna with enhanced isolation for LTE, WiMAX and WLAN mobile handsets," *Electronics Letters*, Vol. 50, No. 10, 723–724, May 8, 2014.
8. Li, J. F., Q. X. Chu, Z. H. Li, and X. X. Xia, "Compact dual band-notched UWB MIMO antenna with high isolation," *IEEE Transactions on Antennas and Propagation*, Vol. 61, No. 9, 4759–4766, Sept. 2013.
9. Addaci, R., A. Diallo, C. Luxey, P. Le Thuc, and R. Staraj, "Dual-band WLAN diversity antenna system with high port-to-port isolation," *IEEE Antennas and Wireless Propagation Letters*, Vol. 11, 244–247, 2012.
10. Morsy, M. M., "2.45 GHz dual polarized aperture-coupled antennas with high isolation performance," *Proceedings of the 2012 IEEE International Symposium on Antennas and Propagation*, 1–2, Chicago, IL, 2012.
11. Kurokawa, K., "Power waves and the scattering matrix," *IEEE Transactions on Microwave Theory and Techniques*, Vol. 13, No. 2, 194–202, Mar. 1965.
12. Rosengren, K. and P. S. Kildal, "Radiation efficiency, correlation, diversity gain and capacity of a six-monopole antenna array for a MIMO system: theory, simulation and measurement in reverberation chamber," *IEE Proceedings — Microwaves, Antennas and Propagation*, Vol. 152, No. 1, 7–16, Feb. 19, 2005.
13. Vaughan, R. G. and J. B. Andersen, "Antenna diversity in mobile communications," *IEEE Transactions on Vehicular Technology*, Vol. 36, No. 4, 149–172, Nov. 1987.
14. Blanch, S., J. Romeu, and I. Corbella, "Exact representation of antenna system diversity performance from input parameter description," *Electronics Letters*, Vol. 39, No. 9, 705–707, May 1, 2003.